INTERNATIONAL JOURNAL FOR NUMERICAL METHODS IN FLUIDS
Int. J. Numer. Meth. Fluids **29**: 827–847 (1999)

NUMERICAL SIMULATION OF THREE-DIMENSIONAL COUETTE–TAYLOR FLOWS

C.B. LIAO[a], S.J. JANE[a] AND D.L. YOUNG[b,*,1]

[a] *Graduate Institute of Civil and Hydraulic Engineering, Feng Chia University, Taichung 407, Taiwan*
[b] *Department of Civil Engineering and Hydrotech Research Institute, National Taiwan University, Taipei 10617, Taiwan*

SUMMARY

To investigate the time-dependent non-axisymmetric flow between two rotating cylinders, or the so-called Couette–Taylor problem, a numerical model to solve the three-dimensional Navier–Stokes equations is established. The projection method is employed to obtain the pressure Poisson equation first. Then the velocity is solved from the equations of motion by using a semi-implicit finite difference scheme. The numerical solution thus obtained has the accuracy of second-order in both time and space discretizations. The Couette–Taylor flow patterns are obtained from direct numerical simulation for the states or regimes of steady circular Couette flow, steady Taylor vortices, and their intermediate processes, as well as also the onset of periodic spiral vortices. The present numerical simulation has also confirmed the location of the transitional boundary of the flow states of the experimental study made by Andereck *et al.* [C.D. Anderek *et al.*, *J. Fluid Mech.*, **164**, 155–183 (1986)] Copyright © 1999 John Wiley & Sons, Ltd.

KEY WORDS: direct numerical simulation; three-dimensional flow; projection method; Couette–Taylor flow problem; spiral vortex flow

1. INTRODUCTION

Motion of fluids between two coaxial rotating cylinders or the so-called Couette–Taylor problem [1–3] is a very classic, fascinating and important subject in fluid mechanics; therefore, for a century, it has drawn a lot of researchers in all aspects of theoretical, computational and experimental investigations. There are several flow regimes existing in an incompressible fluid between two concentric independently rotating cylinders. Hydrodynamic instability and flow transition between states or regimes were determined by the inner and outer cylinder Reynolds numbers Re_1 and Re_2 respectively. The flow regimes in general consist of different spatial and temporal patterns. For time-independent axisymmetric flows, the Couette and Taylor vortex flows are most often observed. There are also non-stationary, non-axisymmetric flows that are more unstable and complex, such as spiral vortex flows, wavy vortex flows, wavy spirals, modulated wavy vortices, twists and turbulent flows, etc. Those flow regimes can be found lucidly from the recent experimental works, e.g. Andereck *et al.* [4].

According to experimental observations of Andereck *et al.*, most flows in general are non-stationary and non-axisymmetric (three-dimensional) in nature, except the simple flow

---

* Correspondence to: Department of Civil Engineering and Hydrotech Research Institute, National Taiwan University, Taipei 10617, Taiwan. Tel.: +886 2 23626114; E-mail: dlyoung@hy.ntu.edu.tw
[1] Fax: +886 2 23639258.

CCC 0271–2091/99/070827–21$17.50

Received December 1997
Revised March 1998

regimes of the circular Couette and Taylor vortex flows. However, most of the early numerical studies are confined to the axisymmetric flow cases only [5–8]. The assumption of axisymmetry in the Couette–Taylor system is an approximate approach in order to simplify the analysis. However, the validity of the existence of axisymmetric flows needs further examination. Since under the phenomena of bifurcation and symmetry breaking to get a more stable state, a flow with certain symmetries may lose some of its symmetric properties when one or more parameter variable crosses some critical value. In the same thinking, a steady flow may become time-dependent, i.e. periodic, aperiodic or chaotic, as far as time symmetry breaking is concerned. Therefore, a model with the axisymmetric assumption *a priori* is very restrictive to describe the more general flow behaviors of this Couette–Taylor problem. A more reasonable approach is to start with a transient 3D form, which will automatically render the subset of the axisymmetric flow patterns, when the axisymmetric characteristics should be maintained.

In this study, a semi-implicit projection method is proposed to solve the unsteady, 3D flow in the cylindrical co-ordinates system (Liao and Young [9]). The numerical code using the finite difference schemes allows the direct numerical simulations for the three regimes of the Couette–Taylor system to be performed. That is, (1) the steady circular Couette flow, (2) the steady axisymmetric Taylor vortex flow, and (3) the periodic spiral vortex flow. These flow patterns of numerical simulation are confirmed with the location of the transitional boundaries of the flow regimes obtained by the experimental observations of Andereck *et al.* Additional flow states are also obtained from this model, such as the modulated wavy vortices. However, due to want of space, it will be reported in another paper.

2. NUMERICAL FORMULATION

2.1. Governing equations

The flow of an incompressible fluid with kinematic viscosity v between two rotating cylinders, of height H and with inner radius r_1 and outer radius r_2, was investigated. The inner cylinder rotates with angular velocity Ω_1 and the outer cylinder rotates with angular velocity Ω_2 respectively. The geometry of the flow in the cylindrical co-ordinates system is shown in Figure 1. The governing equations in dimensionless forms are the continuity and momentum equations as follows:

$$\frac{1}{r}\frac{\partial}{\partial r}(ru)+\frac{1}{r}\frac{\partial v}{\partial \theta}+\frac{\partial w}{\partial z}=0, \tag{1}$$

$$\frac{\partial u}{\partial t}+\frac{1}{r}\frac{\partial}{\partial r}(ruu)+\frac{1}{r}\frac{\partial}{\partial \theta}(vu)+\frac{\partial}{\partial z}(wu)-\frac{v^2}{r}+\frac{\partial p}{\partial r}-\frac{1}{Re}\left[\nabla^2 u-\frac{2}{r^2}\frac{\partial v}{\partial \theta}-\frac{u}{r^2}\right]=0, \tag{2}$$

$$\frac{\partial v}{\partial t}+\frac{1}{r}\frac{\partial}{\partial r}(ruv)+\frac{1}{r}\frac{\partial}{\partial \theta}(vv)+\frac{\partial}{\partial z}(wv)+\frac{uv}{r}+\frac{1}{r}\frac{\partial p}{\partial \theta}-\frac{1}{Re}\left[\nabla^2 v+\frac{2}{r^2}\frac{\partial u}{\partial \theta}-\frac{v}{r^2}\right]=0, \tag{3}$$

$$\frac{\partial w}{\partial t}+\frac{1}{r}\frac{\partial}{\partial r}(ruw)+\frac{1}{r}\frac{\partial}{\partial \theta}(vw)+\frac{\partial}{\partial z}(ww)+\frac{\partial p}{\partial z}-\frac{1}{Re}\nabla^2 w=0, \tag{4}$$

where r, θ and z are the cylindrical co-ordinates with corresponding velocity components u, v and w respectively; p is the dynamic pressure of fluid, t is the time. $Re=r_1\Omega_1 d/v$ is the Reynolds number of the flow, $d=r_2-r_1$ is the gap between two cylinders. $As=H/d$ is the aspect ratio of the cylinder, and

$$\nabla^2 = \frac{1}{r}\frac{\partial}{\partial r}\left(r\frac{\partial}{\partial r}\right) + \frac{1}{r^2}\frac{\partial^2}{\partial\theta^2} + \frac{\partial^2}{\partial z^2}$$

is the Laplacian operator in the cylindrical co-ordinate system.

2.2. Initial condition and boundary conditions

The initial condition is the motionless fluid, i.e.

$$t \leq 0, \quad u = v = w = 0, \quad r_1/d \leq r \leq r_2/d, \quad 0 \leq \theta \leq 2\pi, \quad 0 \leq z \leq As. \tag{5}$$

The boundary conditions are described in the following:

1. On the inner cylinder wall

$$u = 0, \quad v = 1.0, \quad w = 0 \quad \text{on} \quad r = r_1/d, \quad 0 \leq \theta \leq 2\pi, \quad 0 \leq z \leq As. \tag{6}$$

2. On the outer cylinder wall

$$u = 0, \quad v = r_2\Omega_2/r_1\Omega_1, \quad w = 0 \quad \text{on} \quad r = r_2/d, \quad 0 \leq \theta \leq 2\pi, \quad 0 \leq z \leq As. \tag{7}$$

3. On the top and end wall, the periodic condition of the cylinder in z-direction

$$\frac{\partial u}{\partial z} = \frac{\partial v}{\partial z} = w = 0 \quad \text{on} \quad z = 0, \quad As, \quad r_1/d \leq r \leq r_2/d, \quad 0 \leq \theta \leq 2\pi. \tag{8}$$

4. Periodic conditions in the θ-direction

$$\begin{aligned} u(r, \theta, z) &= u(r, \theta + 2n\pi, z), \\ v(r, \theta, z) &= v(r, \theta + 2n\pi, z), \\ w(r, \theta, z) &= w(r, \theta + 2n\pi, z), \\ p(r, \theta, z) &= p(r, \theta + 2n\pi, z). \end{aligned} \tag{9}$$

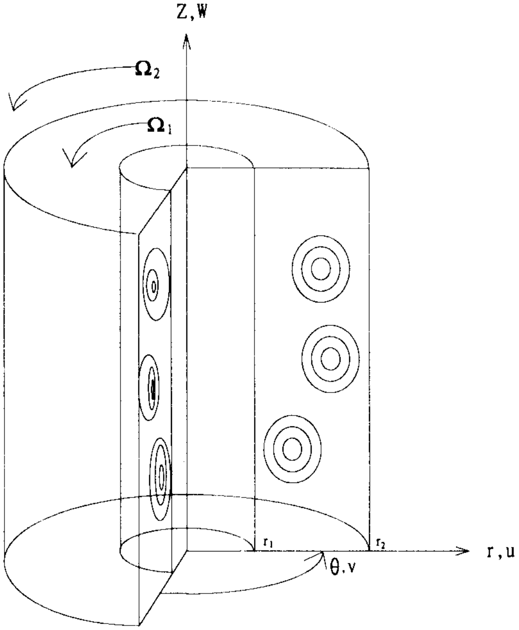

Figure 1. The geometry of the flow in the cylindrical co-ordinates system.

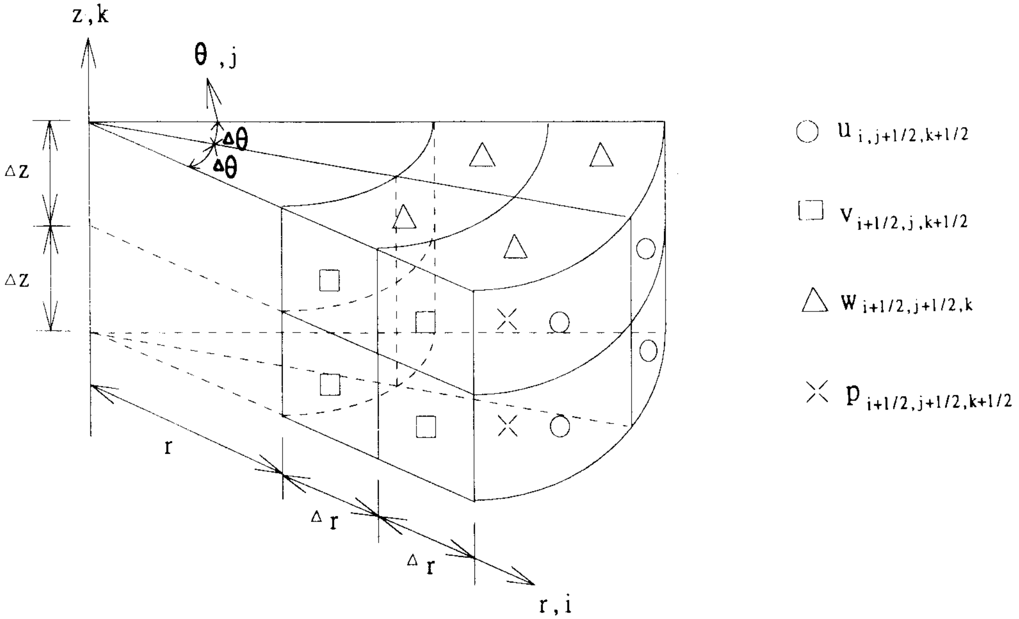

Figure 2. The MAC staggered grid system in the numerical model.

If the flow starts from a motionless fluid with the periodic boundary condition of Equation (8), the radial velocity u, and the axial velocity w, will be zero for all time, except the azimuthal velocity v, in the numerical calculations. To obtain a more complex flow, the introduction of a disturbance is imperative. A simple way to do is to apply the non-slip boundary condition on the end walls first to get the three velocity components, and then replaced by the periodic boundary condition of Equation (8) afterwards to simulate the flow regimes.

2.3. Numerical method

2.3.1. Compound scheme for velocity. The finite difference method is used to solve the governing equations. An implicit Crank–Nicolson scheme is applied to discretize the second derivative terms of θ and an explicit Adams–Bashforth scheme is used to approximate the other terms in the momentum equations. The implicitness of θ discretization is to avoid the excess computational time to overcome the constraint of numerical instability. Thus, momentum equations (Equations (2)–(4)) are discretized as follows:

$$\left[1-\frac{\Delta t}{2\mathrm{Re}r^2}\frac{\delta_\theta^2}{\Delta\theta^2}\right]\left(\frac{u^{n+1}-u^n}{\Delta t}\right)+f^n+\frac{\delta_r}{\Delta r}p^{n+1}=0, \tag{10}$$

$$\left[1-\frac{\Delta t}{2\mathrm{Re}r^2}\frac{\delta_\theta^2}{\Delta\theta^2}\right]\left(\frac{v^{n+1}-v^n}{\Delta t}\right)+g^n+\frac{1}{r}\frac{\delta_\theta}{\Delta\theta}p^{n+1}=0, \tag{11}$$

$$\left[1-\frac{\Delta t}{2\mathrm{Re}r^2}\frac{\delta_\theta^2}{\Delta\theta^2}\right]\left(\frac{w^{n+1}-w^n}{\Delta t}\right)+h^n+\frac{\delta_z}{\Delta z}p^{n+1}=0, \tag{12}$$

where

$$f^n = \frac{3}{2} A^n - \frac{1}{2} A^{n-1} - \frac{1}{Re} \frac{1}{r^2} \frac{\delta_\theta^2}{\Delta\theta^2} u^n,$$

$$g^n = \frac{3}{2} B^n - \frac{1}{2} B^{n-1} - \frac{1}{Re} \frac{1}{r^2} \frac{\delta_\theta^2}{\Delta\theta^2} v^n,$$

$$h^n = \frac{3}{2} C^n - \frac{1}{2} C^{n-1} - \frac{1}{Re} \frac{1}{r^2} \frac{\delta_\theta^2}{\Delta\theta^2} w^n,$$

and

$$A = \frac{1}{r} \frac{\delta_r}{\Delta r} (ruu) + \frac{1}{r} \frac{\delta_\theta}{\Delta\theta} (vu) + \frac{\delta_z}{\Delta z} (wu) - \frac{v^2}{r} - \frac{1}{Re} \left[\frac{1}{r} \frac{\delta_r}{\Delta r} \left(r \frac{\delta_r}{\Delta r} u \right) + \frac{\delta_z^2 u}{\Delta z^2} - \frac{2}{r^2} \frac{\delta_\theta v}{\Delta\theta} - \frac{u}{r^2} \right],$$

$$B = \frac{1}{r} \frac{\delta_r}{\Delta r} (ruv) + \frac{1}{r} \frac{\delta_\theta}{\Delta\theta} (vv) + \frac{\delta_z}{\Delta z} (wv) + \frac{uv}{r} - \frac{1}{Re} \left[\frac{1}{r} \frac{\delta_r}{\Delta r} \left(r \frac{\delta_r}{\Delta r} v \right) + \frac{\delta_z^2 v}{\Delta z^2} + \frac{2}{r^2} \frac{\delta_\theta u}{\Delta\theta} - \frac{v}{r^2} \right]$$

$$C = \frac{1}{r} \frac{\delta_r}{\Delta r} (ruw) + \frac{1}{r} \frac{\delta_\theta}{\Delta\theta} (vw) + \frac{\delta_z}{\Delta z} (ww) - \frac{1}{Re} \left[\frac{1}{r} \frac{\delta_r}{\Delta r} \left(r \frac{\delta_r}{\Delta r} w \right) + \frac{\delta_z^2 w}{\Delta z^2} \right],$$

where δ_r, δ_θ, δ_z are the difference operators, and Δr, $\Delta\theta$, Δz are the grid sizes in r-, θ-, z-directions respectively. Figure 2 shows the marker-and-cell (MAC) staggered grid system that is used in the numerical model.

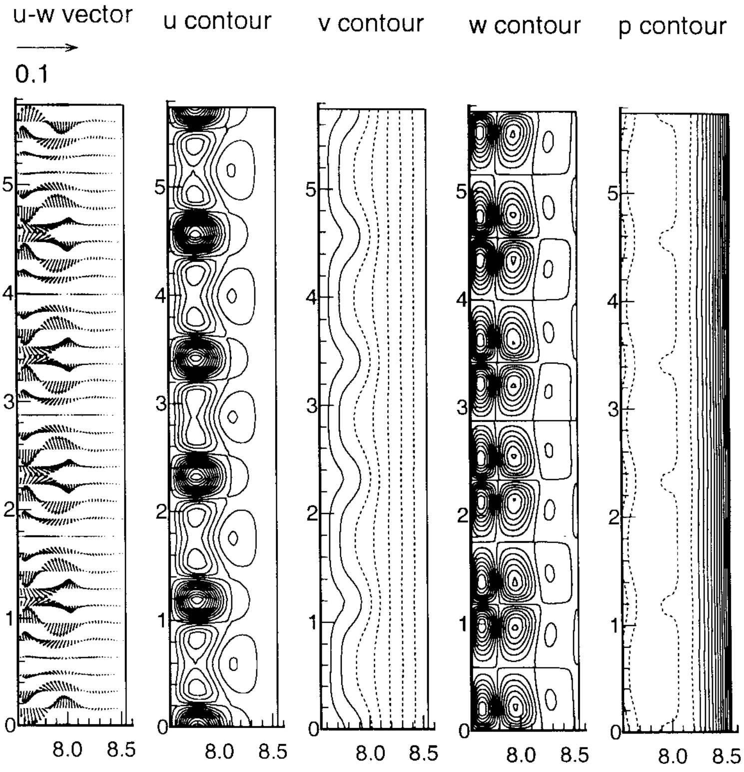

Figure 3. The flow structures of $\boldsymbol{u}$–$\boldsymbol{w}$ vector and u, v, w and p contours on any meridian plane at $t = 400$ for $Re_1 = 350$, $Re_2 = -690$.

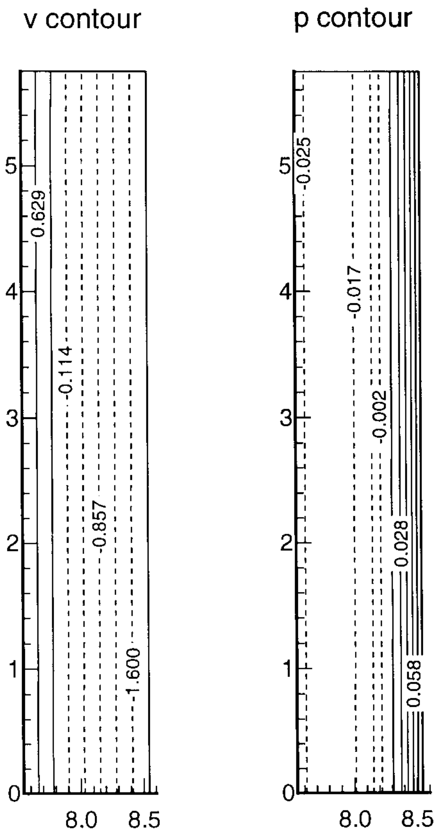

Figure 4. The steady state solution of v and p contours on any meridian plane for $Re_1 = 350$, $Re_2 = -690$.

2.3.2. Semi-implicit projection method for pressure. Taking the divergence to the discretized momentum equations and neglecting some higher-order terms in θ-direction, the pressure Poisson equation is obtained and stated as follows:

$$\frac{1}{r}\frac{\delta_r}{\Delta r}\left(r\frac{\delta_r}{\Delta r}p^{n+1}\right)+\frac{1}{r^2}\frac{\delta_\theta^2}{\Delta\theta^2}p^{n+1}+\frac{\delta_z^2}{\Delta z^2}p^{n+1}$$
$$=\frac{1}{r}\frac{\delta_r}{\Delta r}\left[r\left(\frac{u^n}{\Delta t}-f^n\right)\right]+\frac{1}{r}\frac{\delta_\theta}{\Delta\theta}\left(\frac{v^n}{\Delta t}-g^n\right)+\frac{\delta_z}{\Delta z}\left(\frac{w^n}{\Delta t}-h^n\right), \tag{13}$$

with the Neumann boundary conditions in r- and z-directions as

$$\frac{\delta_r}{\Delta r}p^{n+1}=-\left(\frac{u^{n+1}-u^n}{\Delta t}+f^n\right)\quad \text{on}\quad r=\frac{r_1}{d},\ \text{and} \tag{14a}$$

$$\text{on}\quad r=\frac{r_2}{d}, \tag{14b}$$

$$\frac{\delta_z}{\Delta z}p^{n+1}=-\left(\frac{w^{n+1}-w^n}{\Delta t}+h^n\right)\quad \text{on}\quad z=0,\ \text{and} \tag{14c}$$

$$\text{on}\quad z=As, \tag{14d}$$

and the periodic boundary condition in the θ-direction is

$$p^{n+1}(r, \theta, z) = p^{n+1}(r, \theta + 2n\pi, z). \tag{14e}$$

In the MAC staggered grid system, the boundary conditions Equations (14a)–(14d) are satisfied automatically and are not needed eventually. The detailed procedures will be described as follows:

The discretized differencing equation in the z-direction of Equation (13) at $k = 1/2$ point (first grid point in the z-direction) is

$$\cdots + \frac{1}{\Delta z}\left(\frac{\delta_z}{\Delta z} p^{n+1}_{i+1/2, j+1/2, 1} - \frac{\delta_z}{\Delta z} p^{n+1}_{i+1/2, j+1/2, 0}\right)$$

$$= \cdots + \frac{1}{\Delta z}\left(\left(\frac{w^n}{\Delta t} - h^n\right)_{i+1/2, j+1/2, 1} - \left(\frac{w^n}{\Delta t} - h^n\right)_{i+1/2, j+1/2, 0}\right). \tag{13a}$$

From boundary condition on $z = 0$ of Equation (14c), we have

$$\frac{\delta_z}{\Delta z} p^{n+1}_{i+1/2, j+1/2, 0} = -\left(\frac{w^{n+1} - w^n}{\Delta t} + h^n\right)_{i+1/2, j+1/2, 0}.$$

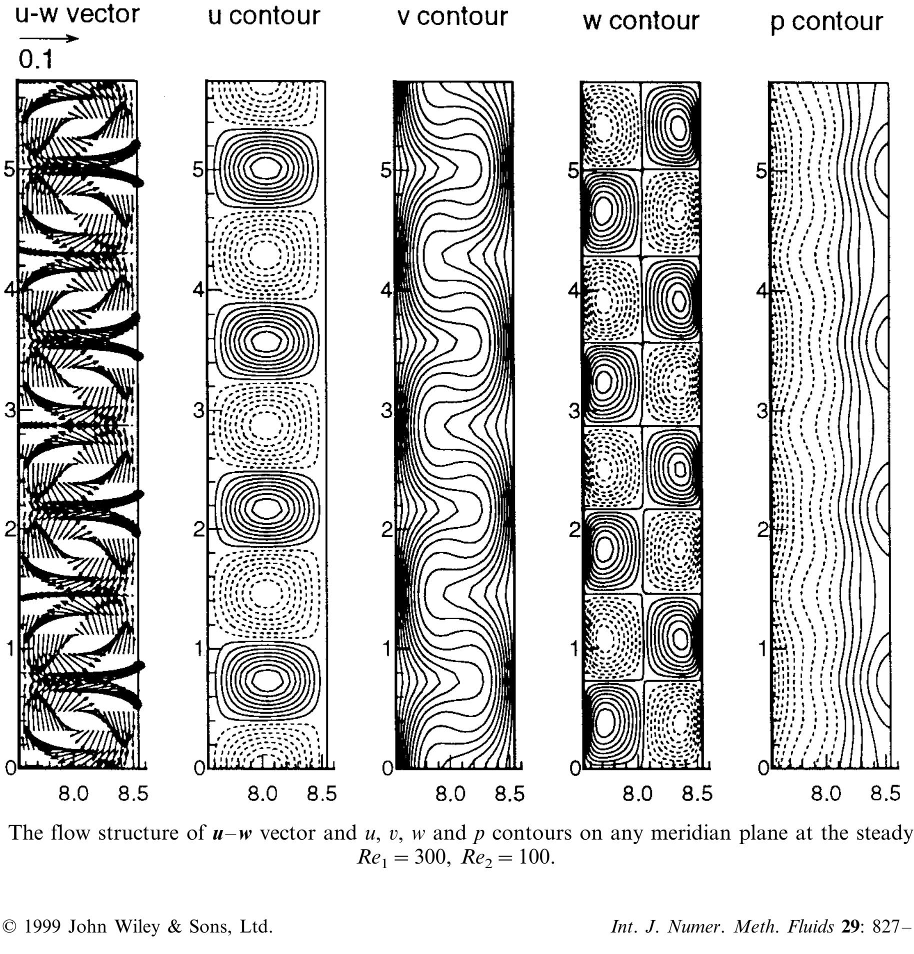

Figure 5. The flow structure of $\boldsymbol{u}$–$\boldsymbol{w}$ vector and u, v, w and p contours on any meridian plane at the steady state for $Re_1 = 300$, $Re_2 = 100$.

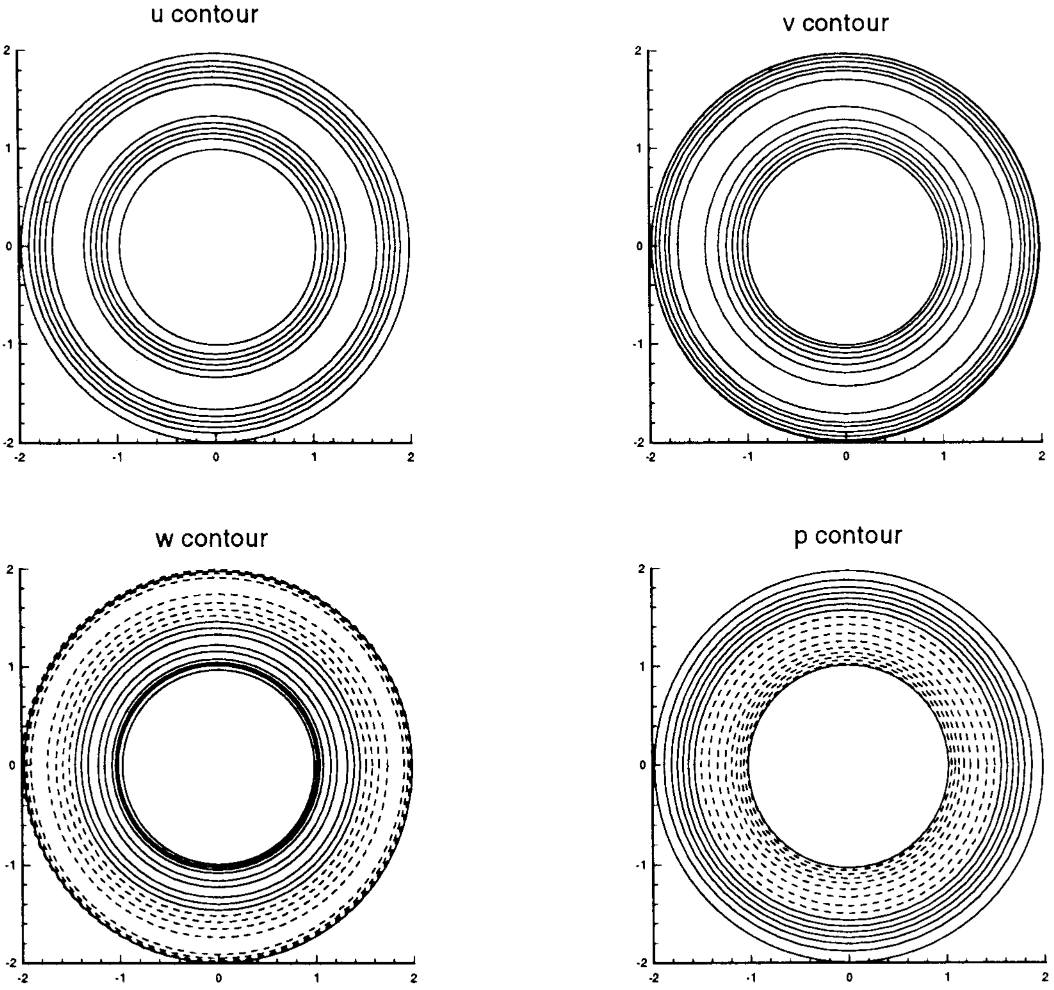
u contour

v contour

w contour

p contour

Figure 6. The steady state solution of u, v, w and p contours at $z = 0.64$ for $Re_1 = 300$, $Re_2 = 100$.

This relation appears in both sides of Equation (13a), therefore, one may take $h^n = 0$ and also $(\delta_z/\Delta z)p = 0$ on $z = 0$ boundary. The remaining three boundary conditions in Equations (14a), (14b) and (14d) are treated by using the same argument. If $f^n = 0$ on $r = r_1/d$ and $r = r_2/d$; $h^n = 0$ on $z = 0$ and $z = As$, then the Equations (14a)–(14d) can be rewritten as

$$\frac{\delta_r}{\Delta r} p^{n+1} = 0 \quad \text{on} \quad r = \frac{r_1}{d}, \text{ and} \tag{15a}$$

$$\text{on} \quad r = \frac{r_2}{d}, \tag{15b}$$

$$\frac{\delta_z}{\Delta z} p^{n+1} = 0 \quad \text{on} \quad z = 0, \text{ and} \tag{15c}$$

$$\text{on} \quad z = As. \tag{15d}$$

Hence p^{n+1} can be solved from the pressure Poisson equation (13) as well as from the boundary conditions (14e) and (15) by using the fast Fourier transform (FFT) and a tridiagonal matrix algorithm (TDMA). The details are described as follows:

Let

$$p^{n+1}_{i+1/2,j+1/2,k+1/2}(r,\theta,z)=\sum_{m=0}^{N-1}\sum_{l=o}^{L-1}a_{ml}(r)\exp(im\theta_{j+1/2})\cos l\pi z_{k+1/2};$$

$$j=0,1,2,\ldots,N-1;\quad k=0,1,2,\ldots,L-1, \tag{16}$$

then the boundary conditions Equations (14e), (15c) and (15d) will be fully satisfied. Expanding the right-hand-side of Equation (13) by

$$R^{n}_{i+1/2,j+1/2,k+1/2}(r,\theta,z)=\sum_{m=0}^{N-1}\sum_{l=0}^{L-1}b_{ml}(r)\exp(im\theta_{j+1/2})\cos l\pi z_{k+1/2};$$

$$j=0,1,2,\ldots,N-1;\quad k=0,1,2,\ldots,L-1. \tag{17}$$

Substituting Equations (16) and (17) into (13), we have

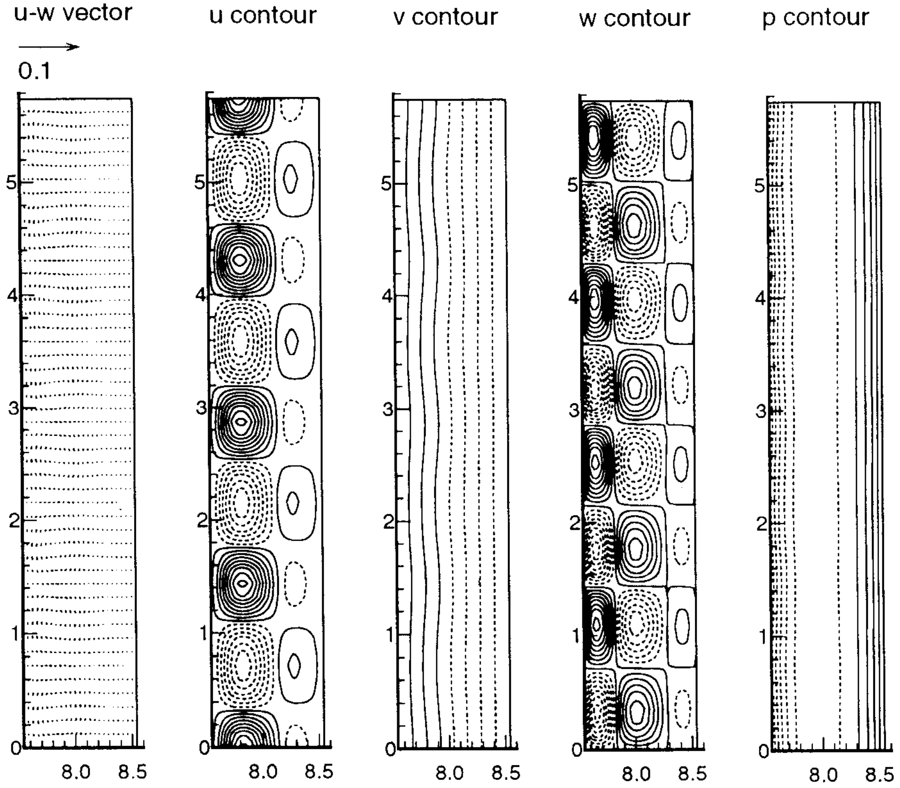

Figure 7. The flow structures of $\boldsymbol{u}$–$\boldsymbol{w}$ vector and u, v, w and p contours on the $\theta=0$ meridian plane at $t=1125.8$ for $Re_1=240$, $Re_2=-300$.

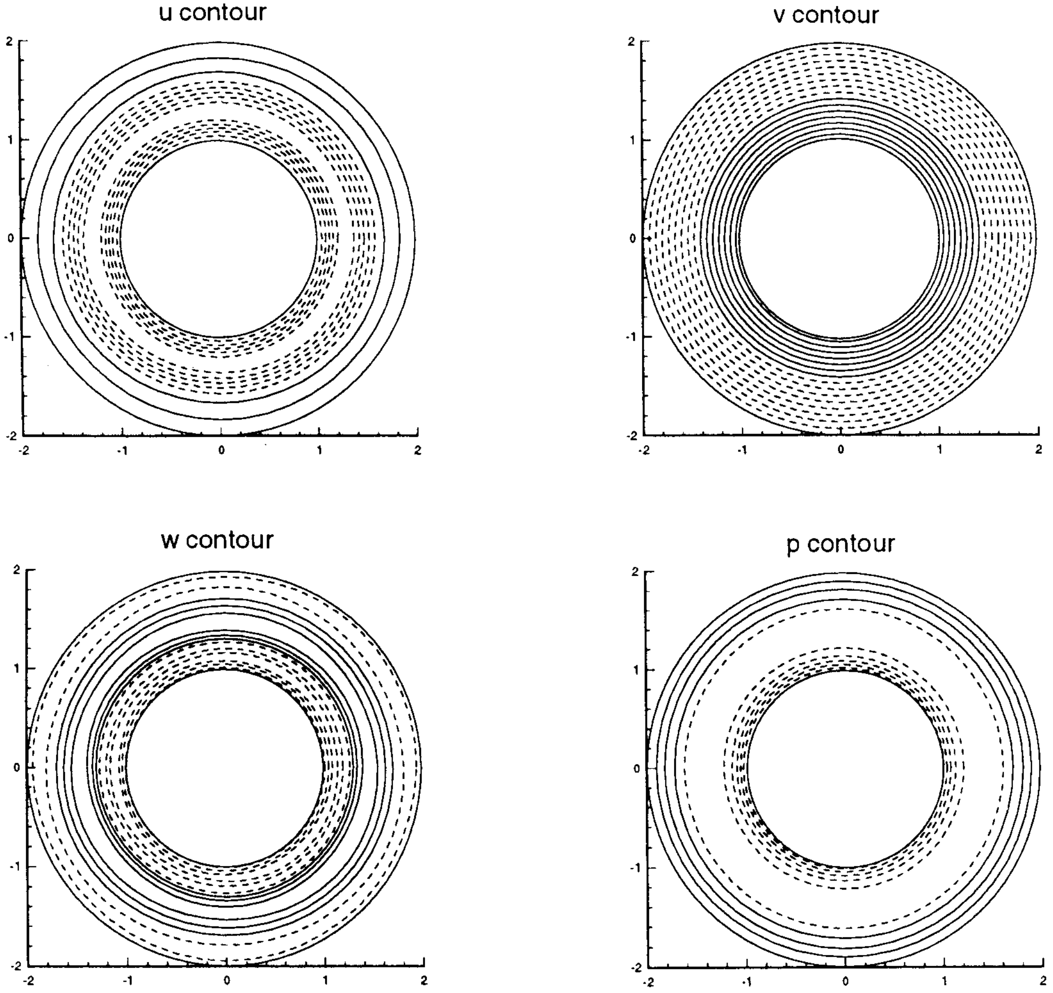

Figure 8. The velocity and pressure contours on the $z = 2.4$ plane at $t = 1125.8$ for $Re_1 = 240$, $Re_2 = -300$.

$$\left[\frac{1}{r}\frac{\delta r}{\Delta r}\left(r\frac{\delta r}{\Delta r}\right) - \frac{4\sin^2 m\pi\Delta\theta}{\Delta\theta^2} - \frac{4\sin^2\dfrac{l\pi\Delta z}{2}}{\Delta z^2}\right]a_{ml}(r) = b_{ml}(r);$$
$$m = 0, 1, 2, \ldots, N-1; \quad l = 0, 1, 2, \ldots, L-1. \tag{18}$$

One can obtain $b_{ml}(r)$ from Equation (17) by the FFT, then solving $a_{ml}(r)$ from Equation (18), which is a tridiagonal matrix system and therefore can be solved easily. Finally, $p^{n+1}(r, \theta, z)$ will be solved from Equation (16) by using the inverse FFT.

The velocities u^{n+1}, v^{n+1} and w^{n+1} can be solved then from the discretized momentum equations (10)–(12) after p^{n+1} were solved from the above algorithm. Since the periodic boundary condition in θ is adopted, the algebraic system for velocity has the following form:

$$\begin{bmatrix} b & c & 0 & 0 & a \\ a & b & c & \ddots & 0 \\ 0 & a & b & \ddots & 0 \\ 0 & \ddots & \ddots & b & c \\ c & 0 & 0 & a & b \end{bmatrix} \begin{Bmatrix} u_1^* \\ u_2^* \\ \vdots \\ \vdots \\ u_N^* \end{Bmatrix} = \begin{Bmatrix} R_1^* \\ R_2^* \\ \vdots \\ \vdots \\ R_N^* \end{Bmatrix}. \tag{19}$$

This system is then solved by a TDMA with some modifications to take care the terms coming from the θ-direction.

The proposed projection method has the following advantages: (1) the continuity equation will be satisfied up to second-order, which is consistent with the requirement of solution accuracy; (2) the numerical solution has second-order accuracy in both time and space discretization; (3) iterating procedures between the pressure and velocity solver are waived, so that a more efficient algorithm is realized.

3. COMPUTATIONS AND DISCUSSION

The numerical simulations for $r_1 = 5.25$ cm, $r_2 = 5.946$ cm and $H = 4.0$ cm, with several different Re_1, and Re_2 were used in this study. This corresponds to the case study of radius ratio $\eta = r_1/r_2 = 0.883$, and aspect ratio $As = 5.75$. The flow states depend on the inner and outer cylinder Reynolds numbers $Re_1 = r_1\Omega_1 d/\upsilon$ and $Re_2 = r_2\Omega_2 d/\upsilon$ respectively. The negative Reynolds numbers represent the clockwise rotating of the cylinder while the positive Reynolds numbers are for counter-clockwise rotating. Three case studies are performed to demonstrate the three different flow regimes: namely, (1) a steady circular Couette flow, (2) a steady

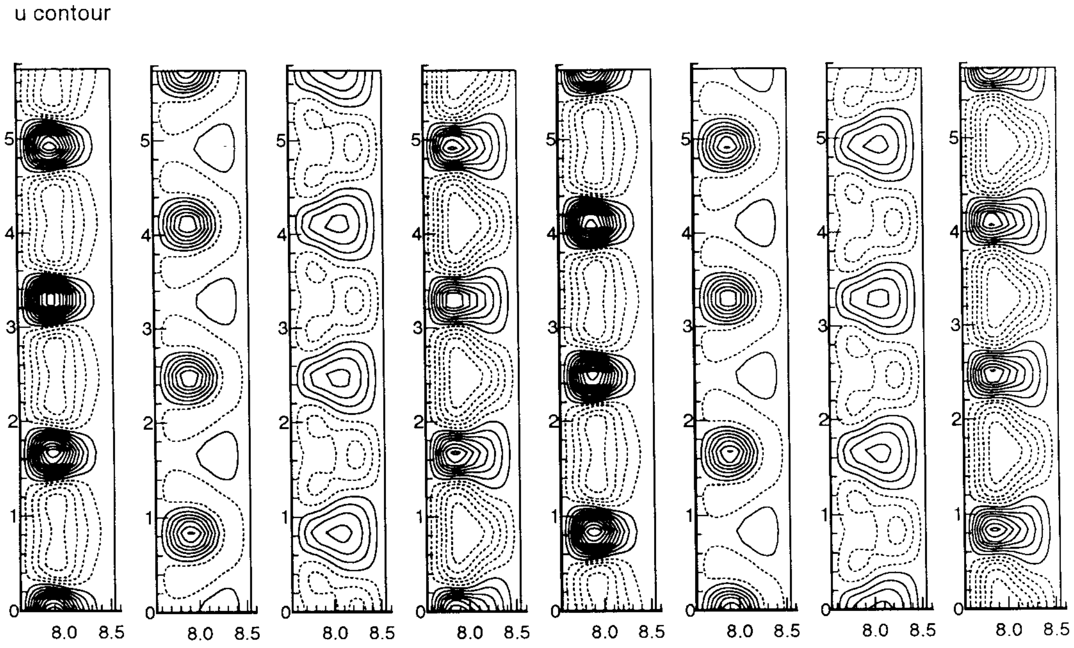

Figure 9. The u contours on the $\theta = 0$, $\pi/4$, $\pi/2$, $3\pi/4$, π, $5\pi/4$, $3\pi/2$, $7\pi/4$ meridian planes at $t = 1751.4$ for $Re_1 = 240$, $Re_2 = -300$.

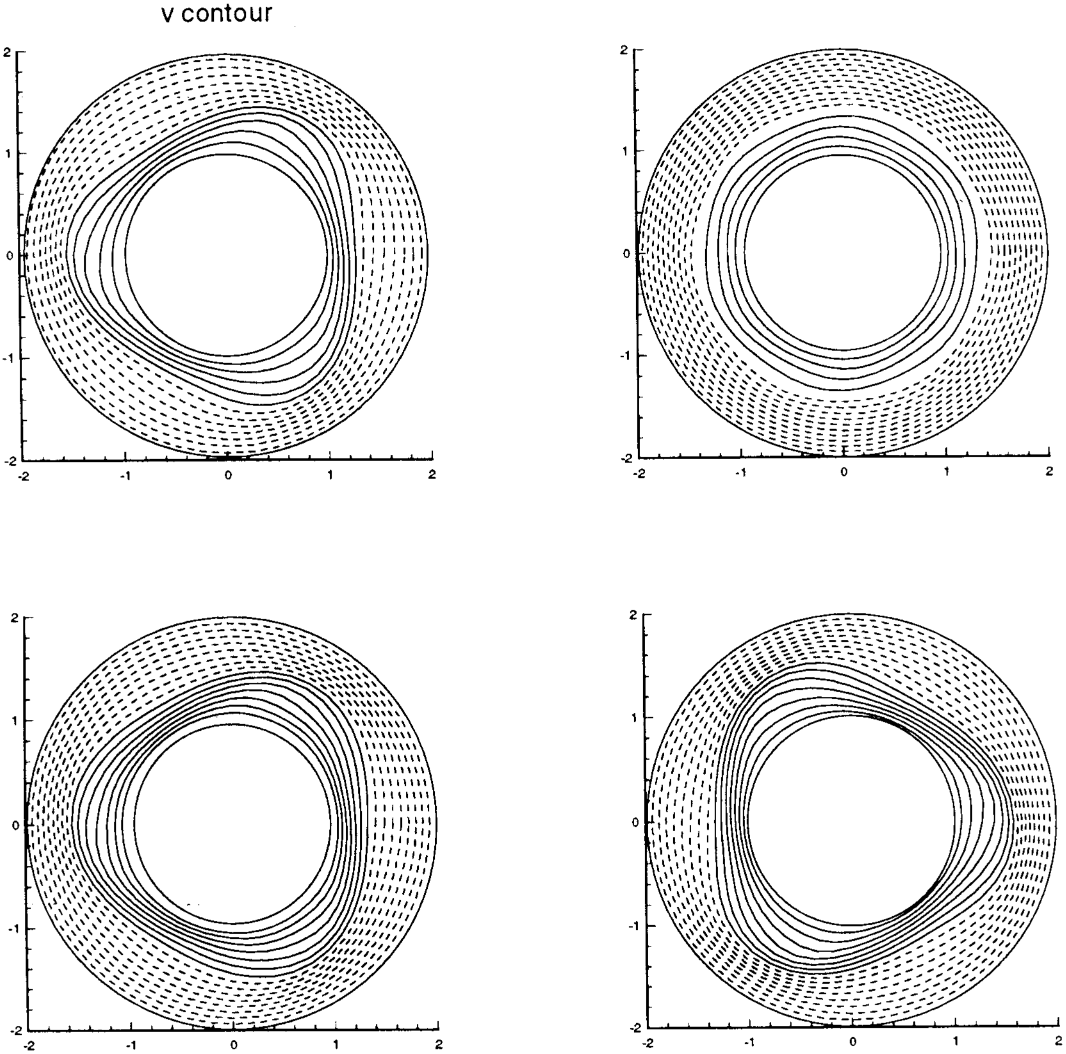

Figure 10. The v contours on the $z = 0.72$, 2.87, 4.31, 5.03 planes at $t = 1751.4$ for $Re_1 = 240$, $Re_2 = -300$.

axisymmetric Taylor vortex, and (3) a periodic spiral vortex flow. This unsteady 3D model will render steady and axisymmetric flow regimes in the long run, as the flow should be steady and axisymmetric in general. Both the salient features of unsteady oscillation in time as well as symmetry breaking in space for the spiral vortices will be illustrated for case (3) in particular.

3.1. Steady circular Couette flow ($Re_1 = 350$, $Re_2 = -690$)

A $72 \times 72 \times 72$ grid and $\Delta t = 0.01$ were adopted for this case study. The flow structures of $\boldsymbol{u}$–$\boldsymbol{w}$ vector, as well as u, v, w, and p contours on any meridian plane (for all θ) at $t = 400$ are shown in Figure 3. At this intermediate stage, five-cell Taylor vortices are observed, the flow pattern is classified as the axisymmetric Taylor vortex flow. However, as the time evolves, the flow finally reaches a steady state solution at $t = 920$. The criterion of the steady state solution is defined by the L_1 norm of the local acceleration being less than 10^{-5}. At this instant, a steady circular Couette flow is realized, which yields the non-zero v component and zero u, w components in the velocity field. The azimuthal velocity consists of a free and a forced vortex, as can be obtained from the analytic solution [10]. Figure 4 exhibits the v and p contours on any meridian plane. From this plot, a steady circular Couette flow pattern is vividly envisaged. It is worthwhile mentioning that the boundary between this Couette flow and spiral flow from the Andereck *et al.* diagram is very close and sensitive in this case study. The sensitivity of the transition boundary between the flow regimes requires cautious measures to be taken in order to get the correct flow pattern, as mentioned in the works of Andereck *et al.*

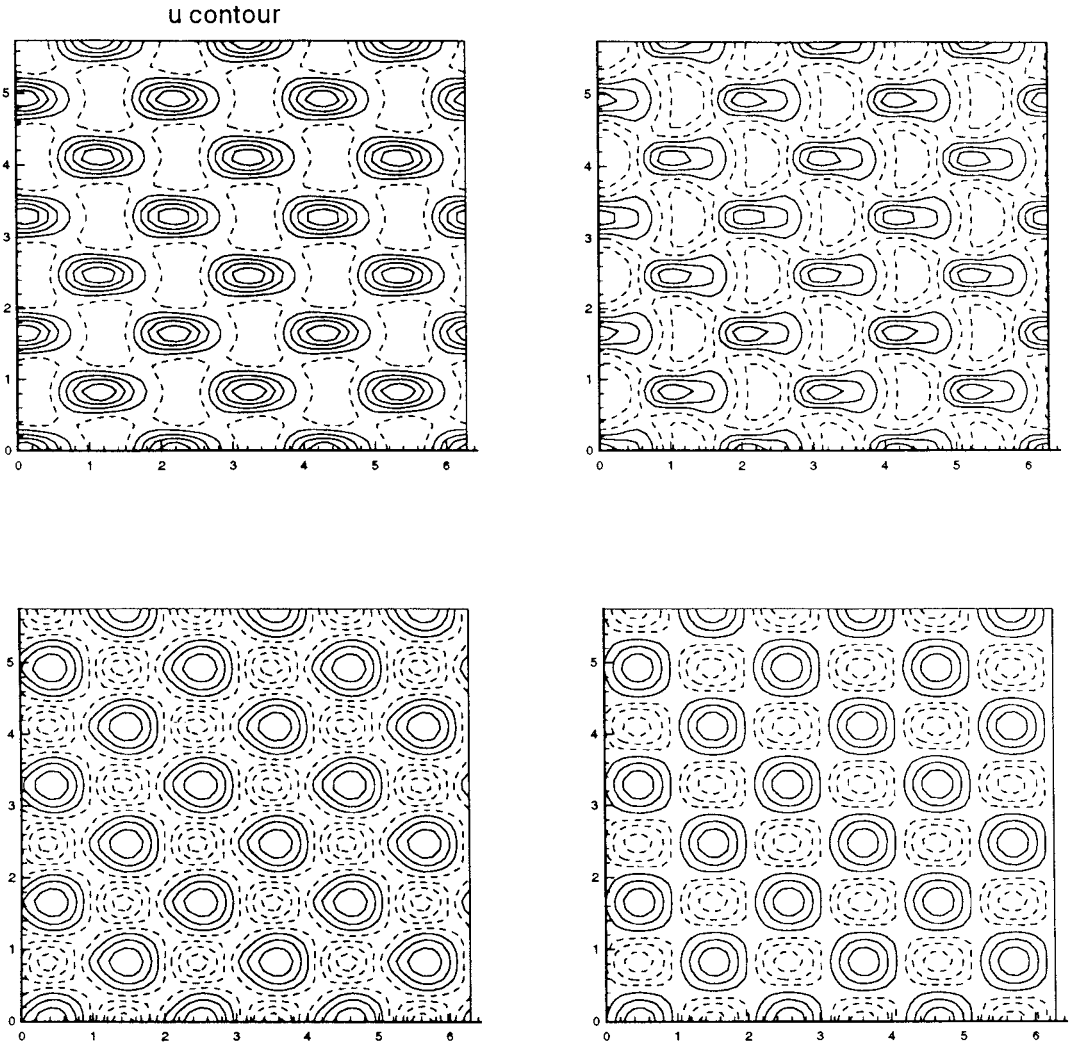

Figure 11. The u contours on $r = 7.67$, 8.04, 8.29, 8.42 circumferential planes at $t = 1751.4$ for $Re_1 = 240$, $Re_2 = -300$.

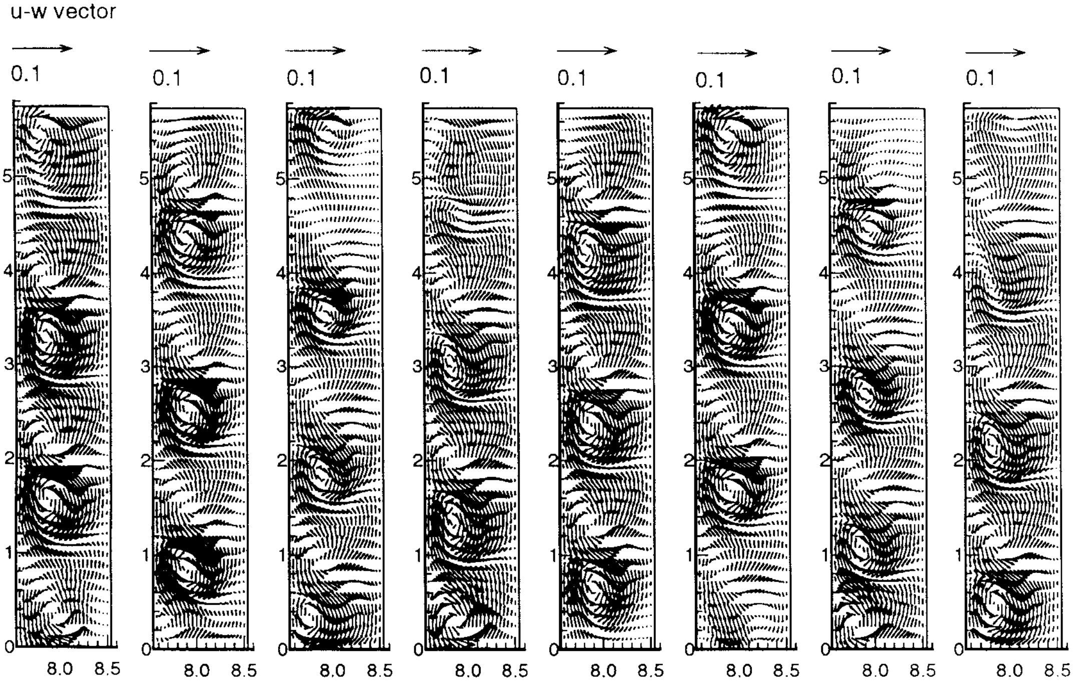

Figure 12. The $\boldsymbol{u}$–$\boldsymbol{w}$ vectors on the $\theta = 0$, $\pi/4$, $\pi/2$, $3\pi/4$, π, $5\pi/4$, $3\pi/2$, $7\pi/4$ meridian planes at $t = 3753.4$ for $Re_1 = 240$, $Re_2 = -300$.

3.2. Steady axisymmetric Taylor vortex flow ($Re_1 = 300$, $Re_2 = 100$)

A $48 \times 48 \times 72$ grid and $\Delta t = 0.01$ were adopted to execute the calculation. The steady state solutions are obtained when $t = 583$ is reached. Figure 5 shows the $\boldsymbol{u}$–$\boldsymbol{w}$ vector and contours of u, v, w, p on any meridian plane. The same flow patterns are obtained for all meridian planes. The axisymmetric property is preserved in this case study, as shown in Figure 6. The figure depicts the contours of u, v, w, the p at horizontal cross-section of $z = 0.64$. It is understood that the gap between the two cylinders is rescaled to magnify the flow structure for easier visualization. This rescaling process is applied in the following similar figures. The Taylor vortices are conspicuously simulated in this case as expected from the theoretical and experimental studies [3,4]. There are four-cell Taylor vortices in this aspect ratio. The flow ends up with a very simple steady and axisymmetric nature, which has been found previously by the Taylor experimental investigations. In the previous numerical studies (Cliffe [6], Cliffe and Mullin [8]), the assumption of symmetry was always introduced to reduce the computational cost. In general, this assumption is restrictive to a simpler flow pattern with the warrant of axisymmetry. However, the present 3D model has the capacity to render the same result for this simple case without the provision of axisymmetric assumption.

3.3. Periodic spiral vortex flow ($Re_1 = 240$, $Re_2 = -300$)

A $48 \times 48 \times 48$ grid system and $\Delta t = 0.01$ were used to simulate the present case. The flow structure lies in the regime of spiral vortex flow as predicted by Andereck *et al.* The corresponding angular velocity of the inner cylinder is $0.596\ \mathrm{s}^{-1}$, while the outer cylinder is $0.656\ \mathrm{s}^{-1}$. Figure 7 displays the flow fields of $\boldsymbol{u}$–$\boldsymbol{w}$ vector and the u, v, w, p contours on any meridian plane at $t = 1125.8$. At this moment, an axisymmetric four-cell Taylor vortex flow prevails. The velocity and pressure contours on the $z = 2.4$ plane are shown in Figure 8. The concentric contours of these flow variables have illustrated that the flow is indeed an axisymmetric Taylor vortex during this transitional period.

However, as time advances further to $t = 1751.4$, the phenomenon of symmetry breaking in the space occurs. The flow is no longer axisymmetric, instead a three-dimensional flow field appears, as revealed from the flow structures of Figures 9–11. The u contours on the $\theta = 0, \pi/4, \pi/2, 3\pi/4, \pi, 5\pi/4, 3\pi/2, 7\pi/4$ meridian planes are portrayed in Figure 9. A 3.5 wavenumber in the axial direction is shown in the figure. The v contours on $z = 0.72$, 2.87, 4.31, 5.03 horizontal planes are depicted in Figure 10. The azimuthal wavenumber is 3 in this numerical computation. Figure 11 shows the u contours on $r = 7.67$, 8.04, 8.29, 8.42 circumferential planes. The alternative arrangement of the vortex cells is displaced horizontally in the

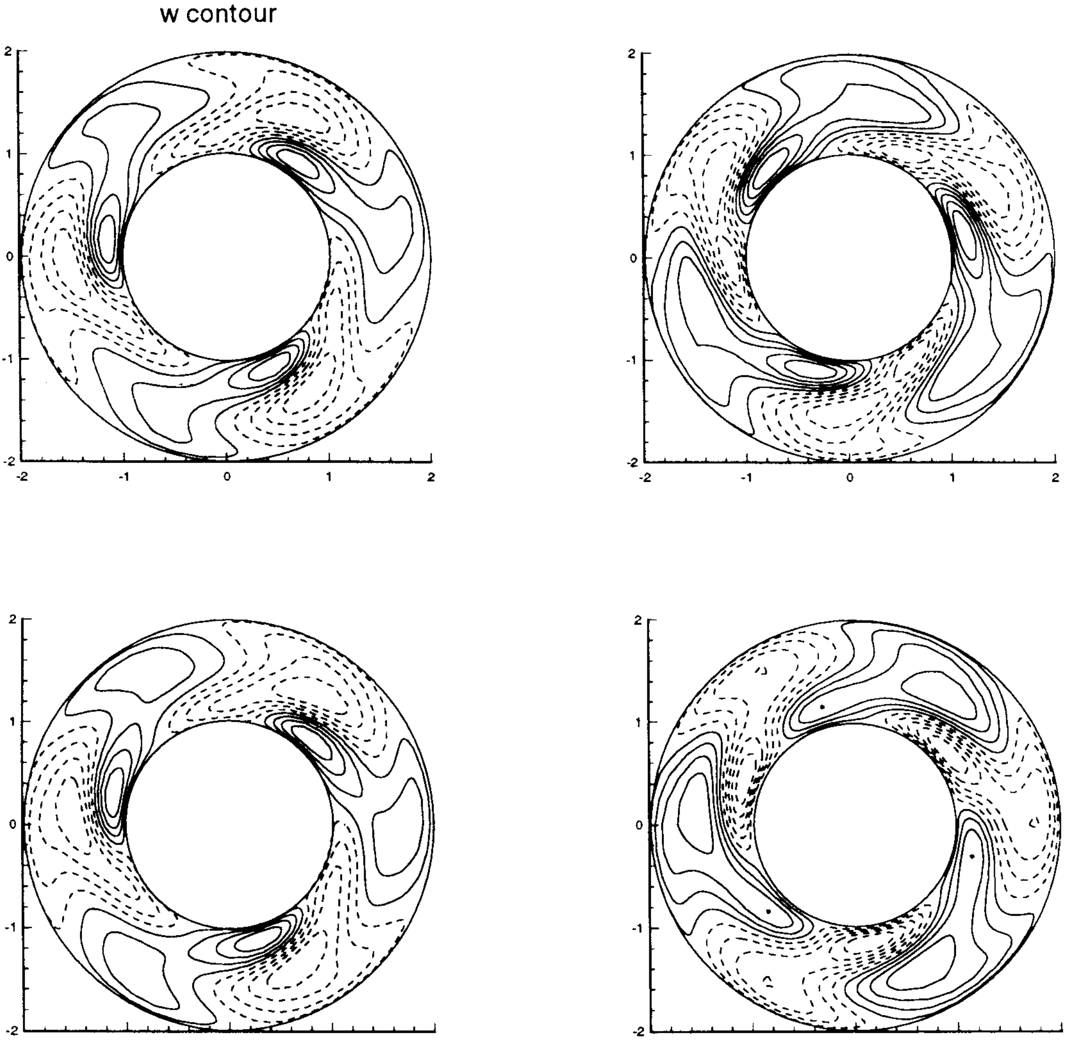

Figure 13. The w contours on the $z = 0.72$, 2.87, 4.31, 5.03 planes at $t = 3753.4$ for $Re_1 = 240$, $Re_2 = -300$.

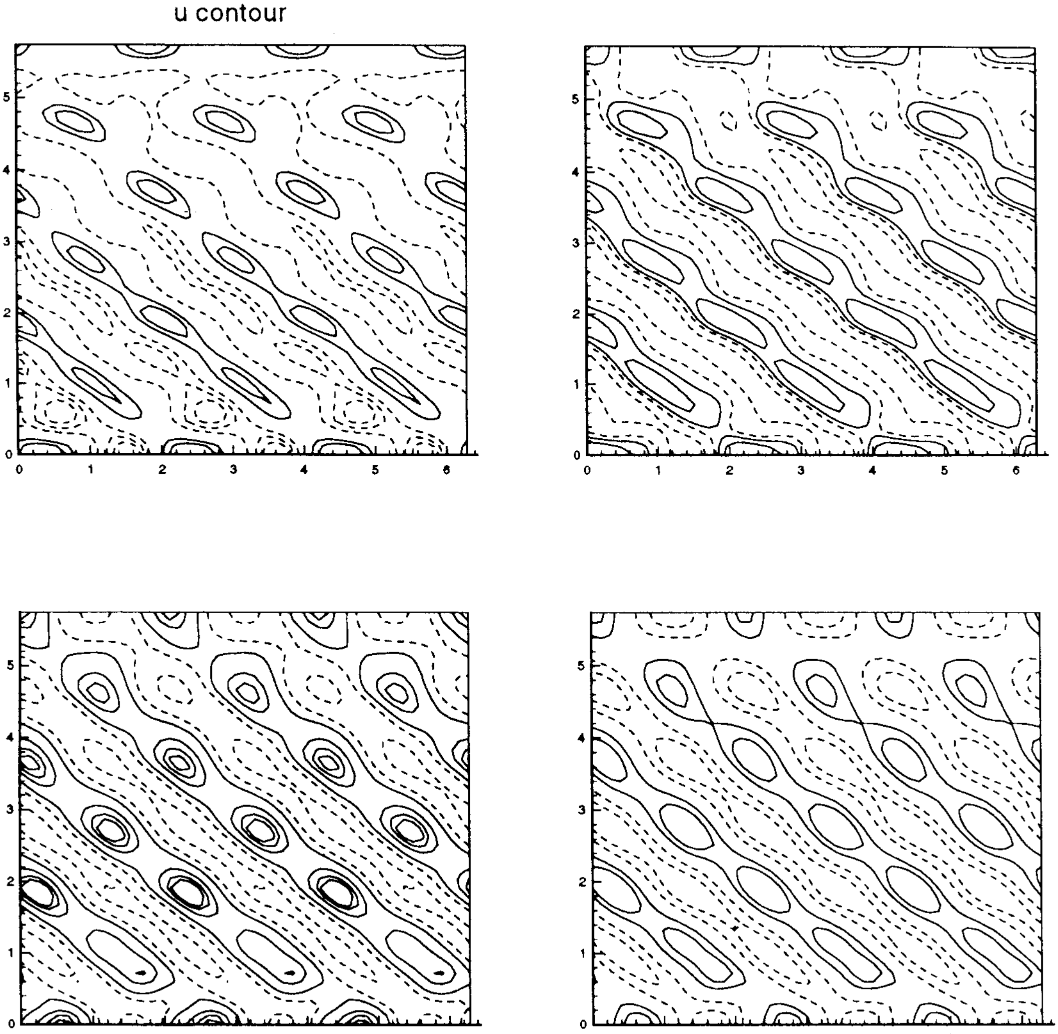

Figure 14. The u contours on $r = 7.67$, 8.04, 8.29, 8.42 circumferential planes at $t = 3753.4$ for $Re_1 = 240$, $Re_2 = -300$.

azimuthal direction. The flow structures of wavenumbers 3.5 in the axial direction and 3 in the azimuthal direction are revealed. The non-axisymmetric character of the flow is also conspicuously demonstrated. However, the formation of the spiral vortex flow is still developing. The non-axisymmetric nature will prohibit the usage of the axisymmetric assumption to simplify the numerical computations.

As the computing process goes on, the flow structures at $t = 3753.4$ are shown in Figures 12–14. Figure 12 illustrates the $\boldsymbol{u}$–$\boldsymbol{w}$ vector on the $\theta = 0$, $\pi/4$, $\pi/2$, $3\pi/4$, π, $5\pi/4$, $3\pi/2$, $7\pi/4$ meridian planes. The spiral structures are revealed from this numerical simulation. The dimensionless axial wavelength is 1.85, and the wavenumber is 3.5 in the axial direction. Figure 13 shows the w contours at $z = 0.72$, 2.87, 4.31, 5.03 horizontal planes. An azimuthal wavenumber of 3 is obtained. The u contours on $r = 7.67$, 8.04, 8.29, 8.42 circumferential

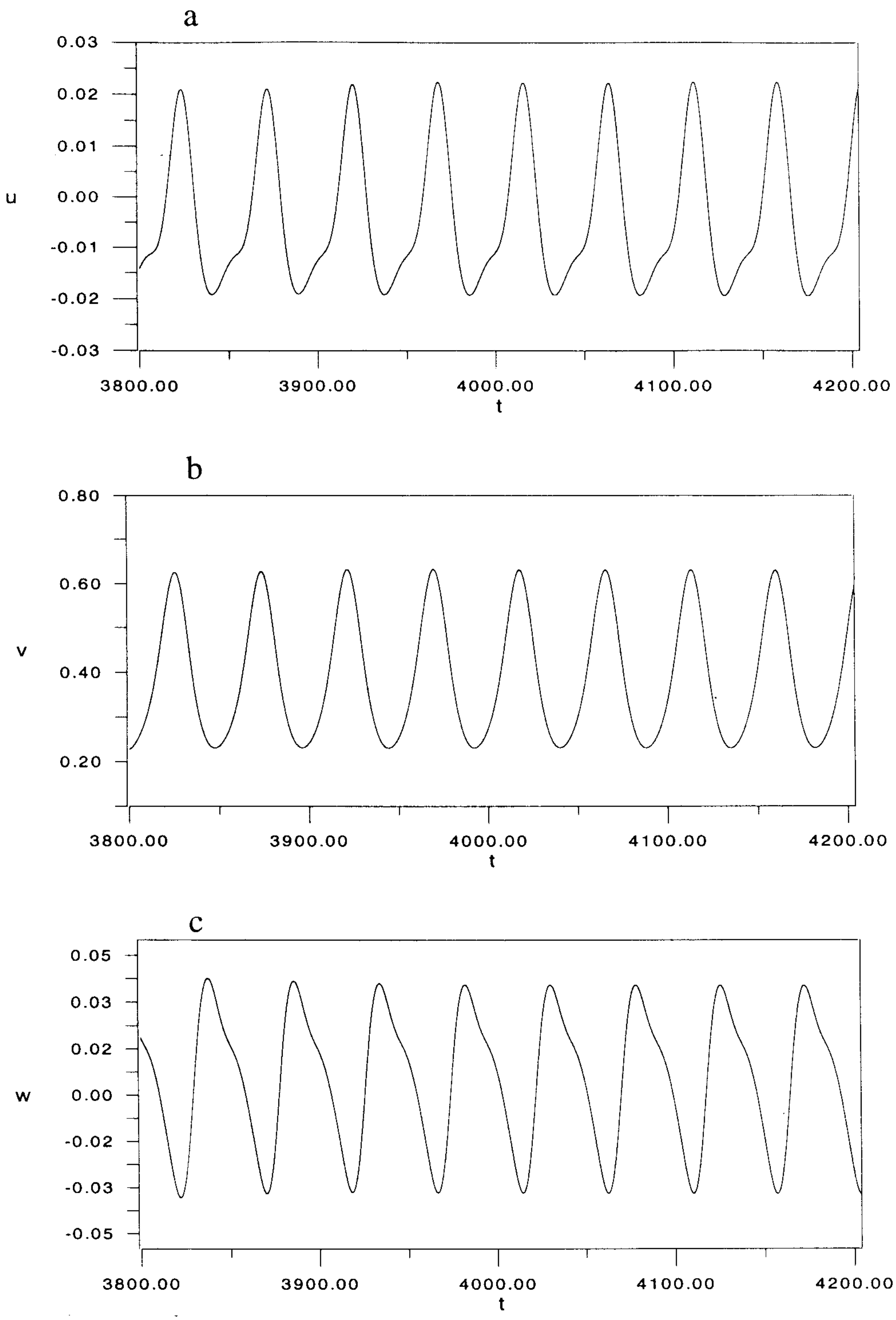

Figure 15. The time histories of u, v and w at the location of (7.8, 1.6, 1.4) for $Re_1 = 240$, $Re_2 = -300$.

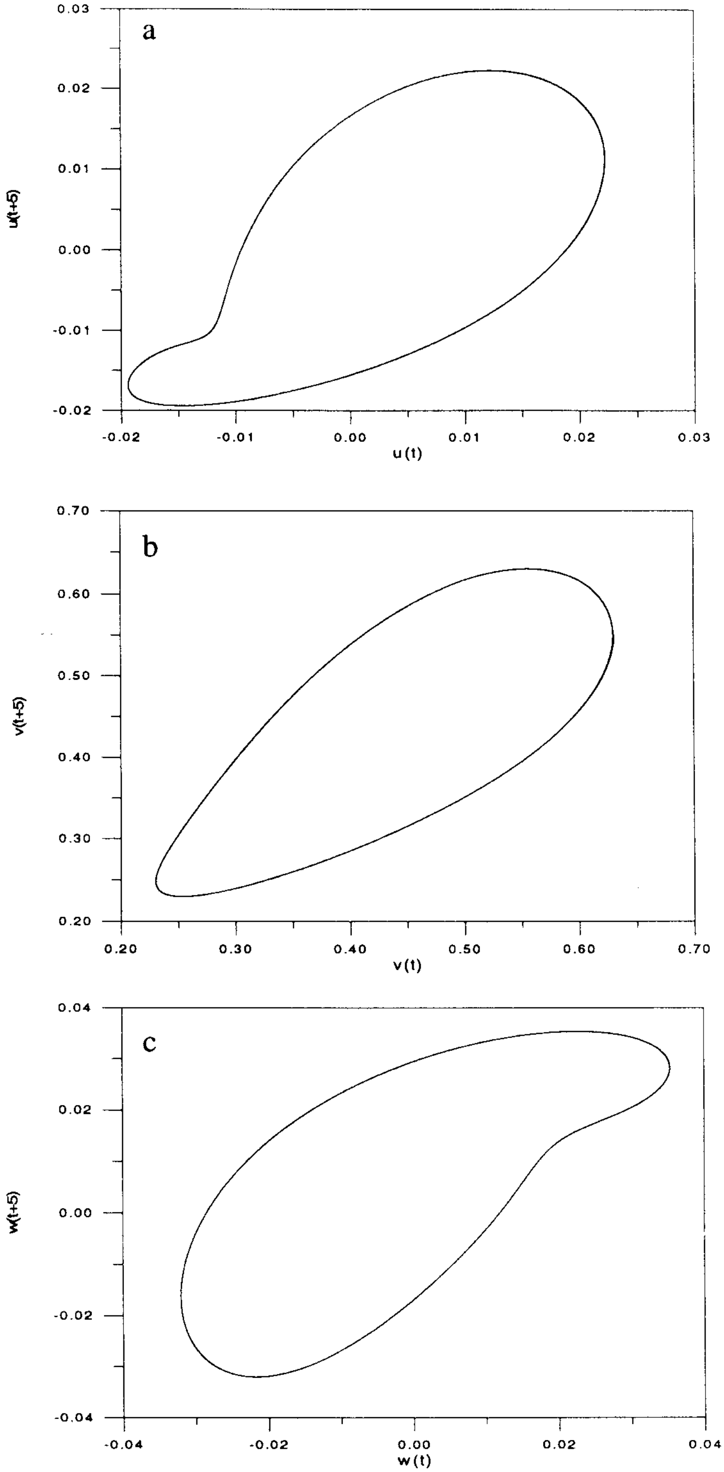

Figure 16. The phase diagrams of the *u*, *v* and *w* components for $Re_1 = 240$, $Re_2 = -300$.

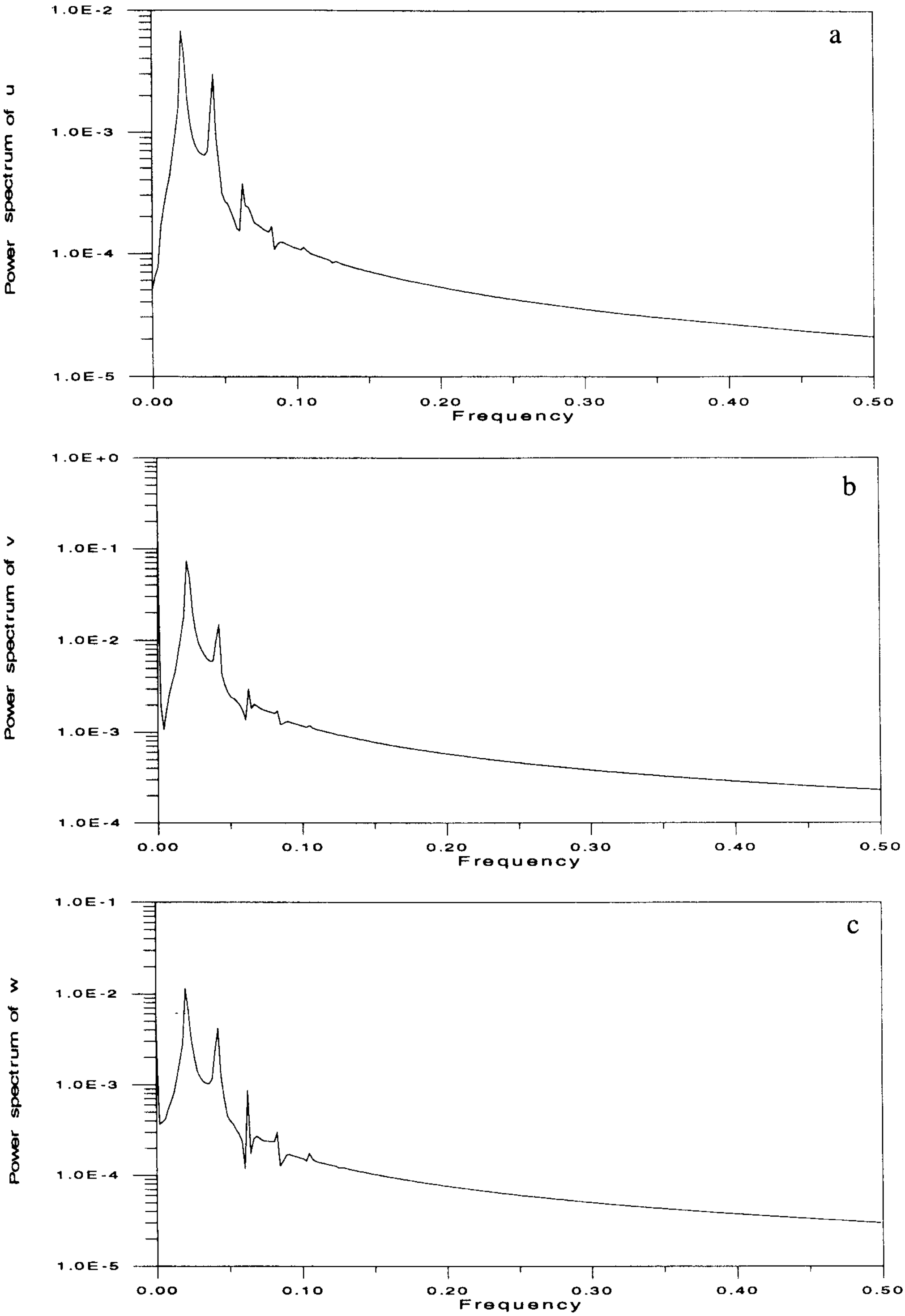

Figure 17. The power spectrum diagrams of the *u*, *v* and *w* component for $Re_1 = 240$, $Re_2 = -300$.

planes are shown in Figure 14. The flow structures are quite different to those of Figure 11. A comparison between Figures 11 and 14 indicates that the horizontal cell structure is transferred to a tilted flow pattern. This phenomenon proves that a spiral vortex is indeed captured.

The evolution of time histories of u, v and w components from $t = 3800$ to $t = 4200$ at the location of (7.8, 1.6, 1.4) is illustrated in Figure 15. The corresponding phase diagrams for each three velocities are depicted in Figure 16. The closed limit cycles for the velocities reveal that the flow is under the category of periodic motion. Further analysis of power spectrum diagrams, as shown in Figure 17 illustrate that there is one major frequency at $f = 0.0208$ in the velocity components. The modulation of the oscillating behavior convinces us that the flow becomes periodic in the long run. The corresponding traveling wave speed for both the axial and azimuthal directions is estimated to be 0.04. From the above mentioned statements, it is concluded that the flow structure evolves from an axisymmetric vortex flow, then to a transitional non-axisymmetric vortex flow, and finally to the periodic laminar spiral vortex flow.

4. CONCLUSIONS

A semi-implicit projection method to solve the unsteady three-dimensional Navier–Stokes equations in the cylindrical co-ordinate system is proposed to undertake the direct numerical simulation of the Couette–Taylor system. Three major flow regimes are achieved, which include the simulations of steady circular Couette flow, steady axisymmetric Taylor vortex flow, and periodic spiral vortex flow. The evolution of intermediate flow structure for each regime transition is also clearly observed on some direct numerical simulation. The locations of the transitional boundaries between flow regimes obtained by experimental study are also reproduced in this investigation. This study has demonstrated the fact that the present unsteady, 3D numerical model can obtain an axisymmeric flow when it has to be axisymmetric such as Couette and Taylor vortex flows, and obtain an unsteady non-axisymmetric flow, such as periodic spiral vortex flow. In short, the present numerical code has the capacity to do the direct numerical simulation for an unsteady, three-dimensional Couette–Taylor flow system. It is concluded that the computational aspect is a useful alternative, in addition to the analytic and experimental studies, to investigate the classic and challenging Couette–Taylor problem.

ACKNOWLEDGMENTS

This study was supported by the National Science Council of the Republic of China, under grant number NSC-85-2211-E-035-014, it is gratefully appreciated. The authors also acknowledged the National Center for High Performance Computing, for supporting the computational work.

APPENDIX A. NOMENCLATURE

As	aspect ratio, $As = H/d$
d	characteristic length, $d = r_2 - r_1$
p	pressure
r	radial co-ordinate

r_1	inner radius
r_2	outer radius
Re	Reynolds number, Re $= r_1\Omega_1 d/v$
Re_1	inner cylinder Reynolds number, Re1 $= r_1\Omega_1 d/v$
Re_2	outer cylinder Reynolds number, Re2 $= r_2\Omega_2 d/v$
t	time
u	radial velocity
v	azimuthal velocity
w	axial velocity
z	axial co-ordinate
η	radius ratio, $\eta = r_1/r_2$
θ	azimuthal co-ordinate
μ	dynamic viscosity
ν	kinematic viscosity
ρ	density of liquid
Ω_1	inner cylinder rotating angular velocity
Ω_2	outer cylinder rotating angular velocity

REFERENCES

1. P. Chossat and G. Iooss, *The Couette–Taylor Problem*, Springer, New York, 1994.
2. M. Couette, 'Etudes sur le frottement des liquides', *Ann. Chim. Phys.*, **6**, 433–510 (1890).
3. G.I. Taylor, 'Stability of a viscous liquid contained between two rotating cylinders', *Philos. Trans. R. Soc. Lond. Ser. A*, **223**, 289–343 (1923).
4. C.D. Andereck, S.S. Liu and H.L. Swinney, 'Flow regimes in a circular Couette system with independent rotating cylinders', *J. Fluid Mech.*, **164**, 155–183 (1986).
5. R. Meyer-Spasche and H.B. Keller, 'Computations of the axisymmetric flow between rotating cylinders', *J. Comp. Phys.*, **35**, 100–109 (1980).
6. K.A. Cliffe, 'Numerical calculations of two-cell and single-cell Taylor flows', *J. Fluid Mech.*, **135**, 219–233 (1983).
7. H. Fasel and O. Booz, 'Numerical investigation of supercritical Taylor vortex flow for a wide gap', *J. Fluid Mech.*, **138**, 21–25 (1984).
8. K.A. Cliffe and T. Mullin, 'A numerical and experimental study of anomalous modes in the Taylor experiments', *J. Fluid Mech.*, **153**, 243–258 (1985).
9. C.B. Liao and D.L. Young, 'A semi-implicit projection method for solving transient 3D flow in cylindrical co-ordinates system', *Proc. 2nd Asian Computational Fluid Dynamics Conference*, Tokyo, Japan, 1996, pp. 319–324.
10. D.J. Tritton, *Physical Fluid Dynamics*, 2nd edn., Oxford University Press, New York, 1988.